
PatchAD: A Lightweight Patch-Based MLP-Mixer for Time Series Anomaly Detection

Zhijie Zhong

South China University of Technology
Guangzhou, China
csemor@mail.scut.edu.cn

Zhiwen Yu

South China University of Technology
Guangzhou, China
zhwyu@scut.edu.cn

Yiyuan Yang*

University of Oxford
Oxford, UK
yiyuan.yang@cs.ox.ac.uk

Weizheng Wang

City University of Hong Kong
Hong Kong, China
weizheng.wang@ieee.org

Kaixiang Yang[†]

South China University of Technology
Guangzhou, China
yangkx@scut.edu.cn

Abstract

Anomaly detection in time series analysis is a pivotal task, yet it poses the challenge of discerning normal and abnormal patterns in label-deficient scenarios. While prior studies have largely employed reconstruction-based approaches, which limits the models' representational capacities. Moreover, existing deep learning-based methods are not sufficiently lightweight. Addressing these issues, we present PatchAD, our novel, highly efficient multiscale patch-based MLP-Mixer architecture that utilizes contrastive learning for representation extraction and anomaly detection. With its four distinct MLP Mixers and innovative dual project constraint module, PatchAD mitigates potential model degradation and offers a lightweight solution, requiring only **3.2MB**. Its efficacy is demonstrated by state-of-the-art results across **9** datasets sourced from different application scenarios, outperforming over **30** comparative algorithms. PatchAD significantly improves the classical F1 score by **50.5%**, the Aff-F1 score by **7.8%**, and the AUC by **10.0%**. The code is publicly available.³

1 Introduction

Time series anomaly detection is a pivotal aspect of data analysis, focused on identifying abnormal patterns within time-series data that significantly deviate from expected behaviour [1, 2, 3]. With the rapid progression of large-scale sensing technologies and storage capabilities, temporal anomaly detection has found widespread application in various sectors. For instance, the Internet of Things (IoTs) serve to monitor abnormal events in sensor data [4, 5]. Unsupervised algorithms, capable of operating without labels, have gained wide popularity. These include reconstruction-based[6, 7], density-based[8, 9], contrastive learning[10, 11], autoregression-based[12, 13, 14], large language

*Work done as an intern at Alibaba Group.

[†]Corresponding author

³<https://github.com/EmorZz1G/PatchAD>

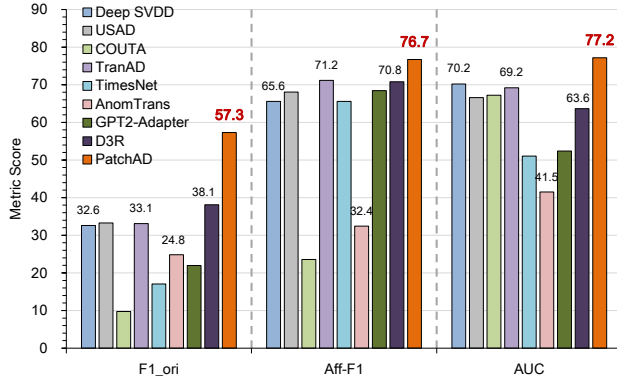


Figure 1: Overall performances under different metrics.

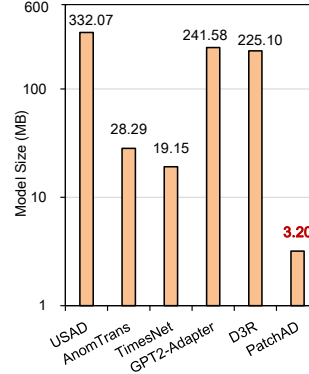


Figure 2: Model sizes.

models (LLMs)[15] *etc.* However, extracting anomalies from extensive and complex temporal data presents significant challenges for different algorithms. **Challenge 1:** Accurately defining anomaly representations is challenging due to real-world anomalies’ diverse and dynamic nature. Effective anomaly detection requires models that can learn the interrelationships between various data channels. **Challenge 2:** There is still significant potential for improvement in terms of training and inference speed, model complexity, and the lack of lightweight features. **Challenge 3:** In an unsupervised setting, the challenge lies in establishing a reliable basis to model normal and anomalous data. Specifically, several algorithms have begun incorporating contrastive learning to enhance model representational capabilities. Nonetheless, these approaches often overlook the design of network structures and model degradation issue of contrastive learning. Additionally, they either do not explicitly model inter-channel dependencies [10] or rely solely on basic MLPs or Transformers that focus on temporal information [16], mainly considering point-level features [17].

On the other hand, we find that normal time series data points exhibit reduced information entropy, indicating higher similarity and correlation among them, whereas anomalies show increased entropy due to difficulties in establishing connections with other points. This difference aids our model in detecting anomalies, ensuring that normal data maintains consistent representations across different views, whereas anomalies do not. This fundamental principle forms the basis of our proposed anomaly detection method.

In response to the above challenges and principles, we introduce **PatchAD**, a lightweight **Patch**-based MLP architecture for time series **Anomaly Detection**. Specifically, proposed *Multi-scale Patching and Embedding* decomposes the input data along the temporal dimension into non-overlapping patches, extracting semantically richer features beyond simple point-level characteristics. Besides, various submodels address various time scales, each focusing on different patch sizes. *Patch Mixer Encoders* are introduced to learn the complex relationships within and between patches and channels. A shared *MixRep Mixer* uniformly represents the feature space, while a *Dual Project Constraint* prevents the model from adopting overly simplistic solutions, thereby enhancing its representational capabilities. In detail, this work makes the following contributions:

- (1) **State-of-the-art Anomaly Detection** (Figure1): We propose a novel contrastive learning-based time series anomaly detection method. PatchAD achieves superior performance on 9 benchmark datasets, surpassing over 30 baselines across various evaluation metrics, with and without prior association.
- (2) **Lightweight and Efficient Design** (Figure2): PatchAD employs a multi-scale patch-based MLP-Mixer architecture with different novel strategies, achieving remarkable efficiency and compactness compared to Transformer-based models.
- (3) **Comprehensive Analysis:** An extensive ablation study validates the effectiveness of each component of PatchAD, supported by a theoretical analysis that elucidates the model’s underlying principles and design choices.

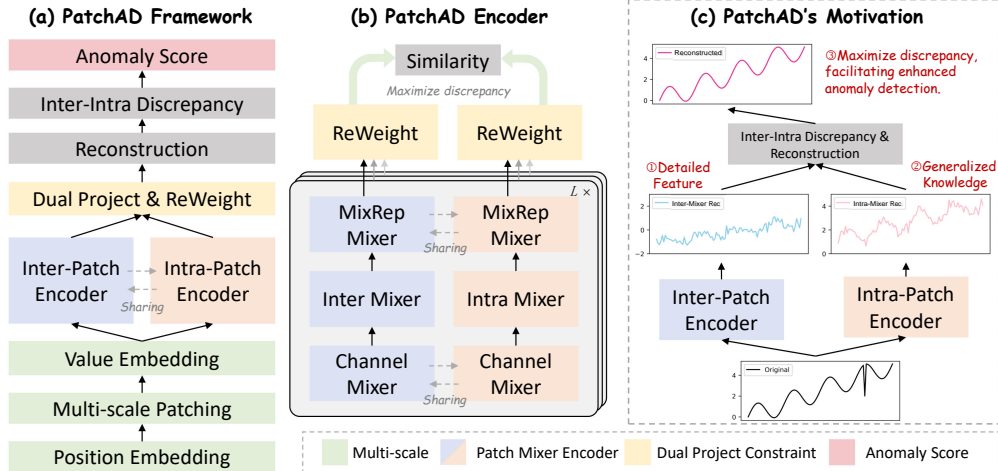


Figure 3: The workflow of the proposed PatchAD framework.

2 Preliminaries

2.1 Problem Formulation

In this paper, we consider a multivariate time series of length T in an unsupervised setting: $\mathcal{X} = (x_1, x_2, \dots, x_T)$, $x_t \in \mathbb{R}^C$ represents a C -dimensional channel feature, such as data from C sensors or machines. The objective is to train a model using \mathcal{X}_{train} and provide predictions $\mathcal{Y}_{test} = (y_1, y_2, \dots, y_{T'})$ on another sequence \mathcal{X}_{test} of length T' . Here, $y_t \in \{0, 1\}$, where 1 signifies an anomaly at that time point and 0 indicates a normal point.

2.2 Time Series Anomaly Detection

The time series anomaly detection methods encompass statistical approaches, classical machine learning methods, and deep learning techniques[18]. Statistical methods involve moving averages and the autoregressive integrated moving average (ARIMA) model. Classical machine learning methods encompass classification-based approaches like One-Class Support Vector Machine (OCSVM) [19] and Support Vector Data Description (SVDD) [20]. Deep learning methods include DAGMM, OmniAnomaly [7], USAD [17], LSTM-VAE [6], and DeepAnT [21], which are trained on normal data and detect anomalies by inference using reconstruction errors. Some techniques have leveraged self-attention mechanisms and have demonstrated promising detection results [22, 23]. While [24] designed six different anomaly injection methods to train the model in a self-supervised approach, [25] utilized outlier exposure and mixup to construct a self-supervised task. Recognizing the limitations imposed by the reconstruction-based assumption, research efforts like [26] introduced sequence variational autoencoder model based on smoothness constraints, whereas [27] proposed prior and sequence associations for temporal modeling, both achieving enhanced performance. Recently approaches based on diffusion models and Large language model have also been proposed [28, 15].

2.3 MLP Mixer & Contrastive Learning for Time Series Analysis

The MLP Mixer initially proposed as a novel architecture for computer vision [29], has gained significant attention in recent years. Recently, there has been analysis indicating that MLP Mixers can effectively handle sequential data and find applications in other domains, such as time series prediction. Specifically, works like [30, 31, 32] have focused on prediction tasks, particularly for multi-step time series prediction, leveraging the capabilities of MLP Mixers to achieve improved forecasting results. Their experiments demonstrate that the MLP Mixer surpasses existing Transformer-based and LSTM-based methods in long sequence time-series forecasting (LSTF).

Contrastive learning aims to drive the model to bring positive pairs closer together in the learned representation space while pushing apart negative pairs. Additionally, methods like BYOL [33] and SimSiam [34] have demonstrated advanced performance without explicitly constructing negative pairs. Recently, studies such as [11] and [35] have explored integrating contrastive learning into time

series analysis. [10], on the other hand, combines self-attention with contrastive learning, achieving state-of-the-art results in time series anomaly detection.

3 Proposed Method

3.1 Overall Architecture

Figure 3 illustrates the overall structure of PatchAD, which adopts patch sizes at multiple scales. We exemplify its architecture using a single scale. PatchAD is an L -layer network, where each layer comprises distinct modules: MLP Mixers, Project head, and ReWeight, forming its structure. We have devised four distinct types of MLP Mixers: Channel Mixer, Inter Mixer, Intra Mixer, and MixRep Mixer, each dedicated to learning various channels, inter-patch, intra-patch relationships, and a unified representation space. The Project head serves to prevent the model from converging to trivial solutions, while the ReWeight module manages the weights across different layers.

The focal point of our design lies in the four distinct MLP Mixers. We utilize various MLP Mixers to learn different representations from the input. Normal points share a common latent space across different views, while anomalies, being scarce and lacking specific patterns, struggle to share a coherent representation with normal points. Consequently, normal points exhibit minor discrepancies across different views, whereas anomalies showcase larger variations. PatchAD leverages inter-intra discrepancy to model this relationship.

Our anomaly detection approach, PatchAD, leverages the principle that normal time series points, characterized by low information entropy, exhibit consistent representations across diverse perspectives. In contrast, anomalies with higher entropy struggle to maintain such consistency (Figure 3(c)). PatchAD employs an Inter-Patch Encoder to capture detailed features and an Intra-Patch Encoder to learn generalized trends. This combined approach enables a comprehensive understanding of normal and anomalous representations, achieving effective anomaly detection.

3.2 Multi-Scale Patching and Embedding

To enhance the temporal contextual representation in time series, we incorporated Transformer positional encoding. Acknowledging the significance of different sequence lengths in the time series analysis, we introduced *Multi-scale Patching* in PatchAD. This enables PatchAD to focus on features of varying sequence lengths. Moreover, incorporating multi-scale information helps compensate for information loss during the patching process. The input data with C channels and length T is transformed into patches of size P . It can be seen as dividing the time series data into N non-overlapping patches, called Patching(\cdot). Thus, the original data of dimensions $C \times T$ is transformed into $C \times N \times P$.

$$\mathcal{X} = \text{Patching}(\text{PE}(\mathcal{X})), \mathcal{X}^{C \times T} \rightarrow \mathcal{X}^{C \times N \times P}, \quad (1)$$

where $\text{PE}(\cdot)$ is positional embedding. PatchAD employs two value embeddings, i.e., $\text{VE}(\cdot)$, facilitating the features from two distinct perspectives within the framework. And $\text{VE}(\cdot)$ is a single linear layer.

$$\begin{aligned} \mathcal{X}_{inter} &= \text{VE}(\mathcal{X}), \mathcal{X}^{C \times N \times P} \rightarrow \mathcal{X}^{C \times N \times D}, \\ \mathcal{X}_{intra} &= \text{VE}(\mathcal{X}), \mathcal{X}^{C \times N \times P} \rightarrow \mathcal{X}^{C \times P \times D}. \end{aligned} \quad (2)$$

3.3 Patch Mixer Encoder

PatchAD comprises L layers of Patch Mixer layers. This encoder incorporates four distinct MLP Mixers to extract features across different dimensions. The MLP Mixer consists of two fully connected layers, a normalization layer and a GELU non-linear activation layer, and utilizes a residual connection from input to output. This can be represented as:

$$\mathcal{X} = \text{FC}(\text{GELU}(\text{FC}(\text{Norm}(\mathcal{X})))) + \mathcal{X}. \quad (3)$$

The following are the different types of MLP Mixers utilized in PatchAD:

1. *Channel Mixer* captures correlations among different channels.
2. *Inter Mixer* captures inter-patch representations, improving detailed expressions.

3. *Intra Mixer* captures intra-patch representations, improving generalized expressions.
4. *MixRep Mixer* embeds two distinct views into the same representation space.

The diagram depicts PatchAD comprised of an inter-patch encoder and an intra-patch encoder, generating representations denoted as $\mathcal{N} \in \mathbb{R}^{C \times N \times D}$ and $\mathcal{P} \in \mathbb{R}^{C \times P \times D}$, representing the inter-patch and intra-patch views, respectively. It’s important to note that *The Channel Mixer* and *The MixRep Mixer* share weights, while *The Inter Mixer* and *The Intra Mixer* have their own weights. This design facilitates PatchAD in learning differences between views and prevents model degradation. In the end, two separate simple MLPs are utilized to reconstruct the original data, which are then combined.

$$\hat{\mathcal{X}}_1 = \text{Rec1}(\mathcal{N}), \quad \hat{\mathcal{X}}_2 = \text{Rec2}(\mathcal{P}), \quad \hat{\mathcal{X}} = \hat{\mathcal{X}}_1 + \hat{\mathcal{X}}_2. \quad (4)$$

3.4 Dual Project Constraint

To prevent the model from converging to trivial solutions, each layer’s output requires to be constrained by *Dual Project Head*. Prior research suggests that employing a similar structure effectively prevents models from converging to trivial solutions. For instance, SimCLR [36] uses a projection head that maps augmented views of an image into a latent space and promotes smoother convergence during training. The projection head comprises two layers of MLP connections, excluding non-linear and normalization layers. Hence, for both the inter-patch and intra-patch encoders, we can derive the projected representations $\mathcal{N}' \in \mathbb{R}^{C \times N \times D}$ and $\mathcal{P}' \in \mathbb{R}^{C \times P \times D}$. This computation can be represented as:

$$\mathcal{N}' = \text{FC}(\text{FC}(\mathcal{N})), \quad \mathcal{P}' = \text{FC}(\text{FC}(\mathcal{P})). \quad (5)$$

To amalgamate outputs from different layers and prevent model degradation, we employ a simple ReWeight module to assign distinct weights to various layers. Considering representations from L layers, $\{\mathcal{N}_1, \mathcal{N}_2, \dots, \mathcal{N}_L\}$ and $\{\mathcal{P}_1, \mathcal{P}_2, \dots, \mathcal{P}_L\}$, we can derive the final result:

$$\begin{aligned} \mathcal{N}_l &= \alpha_l \cdot \mathcal{N}_l, \quad \alpha_l = \text{Softmax}(\alpha), \\ \mathcal{P}_l &= \beta_l \cdot \mathcal{P}_l, \quad \beta_l = \text{Softmax}(\beta). \end{aligned} \quad (6)$$

The introduction of ReWeight allows for a better balance between outputs from different layers, resulting in improved performance.

3.5 Objective Function

The inter-patch encoder and intra-patch encoder can represent two distinct views, denoted as \mathcal{N} and \mathcal{P} . To quantify the dissimilarity between these representations, we utilize a comparative loss function based on Kullback–Leibler divergence (KL divergence), termed as Inter-Intra Discrepancy. Given the scarcity of anomalies in the data and the abundance of normal samples sharing hidden patterns, similar inputs should yield similar representations for both. The loss function for \mathcal{N} and \mathcal{P} can be defined as follows:

$$\begin{aligned} \mathcal{L}_{\mathcal{N}}\{\mathcal{P}, \mathcal{N}\} &= \sum \text{KL}(\mathcal{N}, \text{StopGrad}(\mathcal{P})) + \text{KL}(\text{StopGrad}(\mathcal{P}), \mathcal{N}), \\ \mathcal{L}_{\mathcal{P}}\{\mathcal{P}, \mathcal{N}\} &= \sum \text{KL}(\mathcal{P}, \text{StopGrad}(\mathcal{N})) + \text{KL}(\text{StopGrad}(\mathcal{N}), \mathcal{P}), \end{aligned} \quad (7)$$

where $\text{KL}(\cdot||\cdot)$ represents the KL divergence distance, and StopGrad denotes gradient stoppage, employed for asynchronously optimizing the two branches. The combined loss is defined as:

$$\mathcal{L}_{cont} = \frac{\mathcal{L}_{\mathcal{N}} - \mathcal{L}_{\mathcal{P}}}{\text{len}(\mathcal{N})}. \quad (8)$$

Due to the mismatch in dimensions between \mathcal{N} and \mathcal{P} , an initial upsampling of both is required for comparability. For the inter-patch view, where only differences between patches exist, we replicate the final \mathcal{N} within patches. Conversely, for the intra-patch view, exhibiting anomalies between points within patches, we replicate it multiple times to obtain the final \mathcal{P} . This also addresses the necessity for introducing multi-scale, as it compensates for the information loss during upsampling.

To prevent model degradation, we augment the original loss function with an additional constraint from the projection head, defined as:

$$\mathcal{L}_{proj} = \frac{\mathcal{L}_{\mathcal{N}'} - \mathcal{L}_{\mathcal{P}'}}{\text{len}(\mathcal{N}')} + \frac{\mathcal{L}_{\mathcal{N}} - \mathcal{L}_{\mathcal{P}'}}{\text{len}(\mathcal{N})}. \quad (9)$$

Table 1: Comprehensive comparative results on four datasets. The P, R and F1 are the precision, recall and F1-score. All results are in %, the best in **Bold**, and the second in underlined.

Dataset	MSL			SMAP			PSM			SWaT			Average
	P	R	F1	P	R	F1	P	R	F1	P	R	F1	
OCSVM [19]	59.78	86.87	70.82	53.85	59.07	56.34	62.75	80.89	70.67	45.39	49.22	47.23	61.27
IForest [37]	53.94	86.54	66.45	52.39	59.07	55.53	76.09	92.45	83.48	49.29	44.95	47.02	63.12
LOF [8]	47.72	85.25	61.18	58.93	56.33	57.60	57.89	90.49	70.61	72.15	65.43	68.62	64.50
U-Time [38]	57.20	71.66	63.62	49.71	56.18	52.75	82.85	79.34	81.06	46.20	87.94	60.58	64.50
ITAD [39]	69.44	84.09	76.07	82.42	66.89	73.85	72.80	64.02	68.13	63.13	52.08	57.08	68.78
DAGMM [9]	89.60	63.93	74.62	86.45	56.73	68.51	93.49	70.03	80.08	89.92	57.84	70.40	73.40
VAR [12]	74.68	81.42	77.90	81.38	53.88	64.83	90.71	83.82	87.13	81.59	60.29	69.34	74.80
MMPCACD [40]	81.42	61.31	69.95	88.61	75.84	81.73	76.26	78.35	77.29	82.52	68.29	74.73	75.93
CL-MPPCA [41]	73.71	88.54	80.44	86.13	63.16	72.88	56.02	99.93	71.80	76.78	81.50	79.07	76.05
TS-CP2 [42]	86.45	68.48	76.42	87.65	83.18	85.36	82.67	78.16	80.35	81.23	74.10	77.50	79.91
BeatGAN [43]	89.75	85.42	87.53	92.38	55.85	69.61	90.30	93.84	92.04	64.01	87.46	73.92	80.78
LSTM-VAE [6]	85.49	79.94	82.62	92.20	67.75	78.10	73.62	89.92	80.96	76.00	89.50	82.20	80.97
BOCPD [44]	80.32	87.20	83.62	84.65	85.85	85.24	80.22	75.33	77.70	89.46	70.75	79.01	81.39
Deep-SVDD [45]	91.92	76.63	83.58	89.93	56.02	69.04	95.41	86.49	90.73	80.42	84.45	82.39	81.44
LSTM [46]	85.45	82.50	83.95	89.41	78.13	83.39	76.93	89.64	82.80	86.15	83.27	84.69	83.71
OmniAnomaly [7]	89.02	86.37	87.67	92.49	81.99	86.92	88.39	74.46	80.83	81.42	84.30	82.83	84.56
InterFusion [47]	81.28	92.70	86.62	89.77	88.52	89.14	83.61	83.45	83.52	80.59	85.58	83.01	85.57
THOC [48]	88.45	90.97	89.69	92.06	89.34	90.68	88.14	90.99	89.54	83.94	86.36	85.13	88.76
AnomalyTrans [27]	91.92	96.03	93.93	93.59	99.41	<u>96.41</u>	96.94	97.81	97.37	89.79	100.0	94.62	95.58
DCdetector [10]	92.22	97.48	94.77	94.43	98.41	96.38	97.19	98.08	97.63	93.25	100.0	96.51	96.32
TimesNet [14]	89.54	75.36	81.84	90.14	56.40	69.39	98.51	96.20	97.34	90.75	95.40	93.02	85.40
PatchTST [49]	88.34	70.96	78.70	90.64	55.46	68.82	98.84	93.47	96.08	91.10	80.94	85.72	82.33
GPT2-Adapter [15]	82.00	82.91	82.45	90.60	60.95	72.88	98.62	95.68	97.13	92.20	96.34	94.23	86.67
NPSR-pt [50]	10.60	100.0	19.16	24.99	96.37	39.68	27.74	100.0	43.43	12.29	100.0	21.89	31.04
NPSR-seq [50]	17.66	100.0	30.02	12.79	100.0	22.68	37.87	<u>99.95</u>	54.81	86.76	88.58	87.66	48.80
PatchAD (Ours)	<u>92.05</u>	<u>98.20</u>	95.02	94.49	<u>99.13</u>	96.75	97.72	98.52	98.11	93.28	100.0	96.52	96.60

The final PatchAD loss comprises the two aforementioned components and the reconstruction term ($\mathcal{L}_{rec} = \text{MSE}(\hat{\mathcal{X}}, \mathcal{X})$), which is accompanied by a constraint coefficient to regulate the strength of the constraint.

$$\mathcal{L} = (1 - c) \cdot \mathcal{L}_{cont} + c \cdot \mathcal{L}_{proj} + \mathcal{L}_{rec}. \quad (10)$$

3.6 Anomaly Score

Based on the assumption that normal points across different views share hidden patterns, while anomalies exhibit larger discrepancies, the difference between the two views can be employed as an anomaly score. The final anomaly score can be expressed as:

$$\text{AnomalyScore}(\mathcal{X}) = \sum \text{KL}(\mathcal{N}, \mathcal{P}) + \text{KL}(\mathcal{P}, \mathcal{N}). \quad (11)$$

Based on the aforementioned anomaly score, we set a hyperparameter σ to determine whether a point is considered an anomaly. If it surpasses the threshold, it is identified as an outlier.

4 Experiments

4.1 Setups and Evaluation Metrics

We applied eight multivariable and one univariable datasets for evaluation: (1) MSL (2) SMAP (3) PSM (4) SMD (5) SWaT (6) WADI (7) NIPS-TS-SWAN (8) NIPSTS-GECCO (9) UCR. Details about these datasets are outlined in Table 4 in Appendix. Also, implementation and pseudo-code Algorithm 1 details in Appendix.

We compared our model with several benchmark models, including: (1) Reconstruction-based; (2) Autoregression-based; (3) Density-based; (4) Clustering-based; (5) Classic methods; (6) Change point detection and time-series segmentation methods; (7) Transformer-based methods; (8) Large language model; (9) Diffusion model; See details in Table 1 and Table 5, or in Appendix B.2.

Additionally, we employed various evaluation metrics for assessing, encompassing commonly used metrics in time-series anomaly detection such as AUC, accuracy, precision, recall, F1-score with point adjustment (F1), and original F1-score (F1_ori) [27]. Moreover, we adopted state-of-the-art evaluation techniques like affiliation precision and affiliation recall [51], along with Volume under the surface (VUS) [52]. Although the F1-score is a widely used metric, it does not effectively

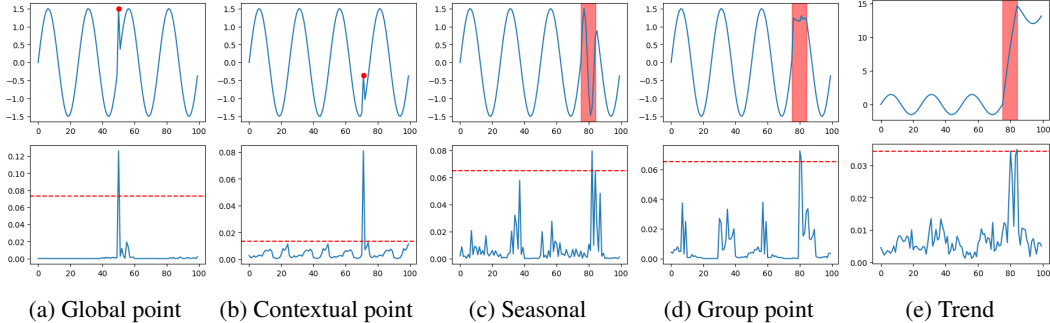


Figure 4: Visualization of generated synthetic data, PatchAD anomaly scores and ground truth.

evaluate anomalous events. Therefore, we introduce the following two new metrics. Affiliation precision and recall are evaluation metrics based on the proximity of predicted events to the true labels. VUS considers including anomalous events in its evaluation by computing the receiver operator characteristic (ROC) curve. Employing various methodologies allows for a more comprehensive evaluation of our model. To compare with other methods fairly, we utilized the point adjustment technique, identifying an anomalous segment if the model detects any anomaly point within the segment.

4.2 Comparison Results

Data Source Clarification: Due to substantial device variations, to ensure a fair comparison with anomaly transformer (AnomalyTrans) and DCdetector, all results mentioned in the paper concerning them are obtained through our reimplementations of their codes. The results of AnomalyTrans and DCdetector in Table 1 and Table 5 are our reproductions.

From Table 1, PatchAD achieves the best average-level F1 performance. As far as we know, there is ongoing controversy regarding the evaluation of time series anomaly detection. However, precision, recall, and F1-score remain the most widely used evaluation metrics. To comprehensively assess the performance of our approach, additional metrics such as affiliation precision/recall and VUS have been introduced.

In Table 5 in Appendix, the NIPS-TS-SWAN and NIPS-TS-GECCO datasets represent more challenging datasets, encompassing a wider array of anomaly types. Compared to other baseline methods, PatchAD consistently achieves SOTA results on these two datasets. Particularly noteworthy is the 9.3% increase in F1-score over the DCdetector and a 24.9% increase over the Anomaly Transformer on the NIPS-TS-GECCO dataset. Given the remarkable performance of AnomalyTrans and DCdetector surpassing other baselines significantly, we conducted a comprehensive comparison of PatchAD with them across all datasets using multiple metrics, as depicted in Table 7 in Appendix. Our proposed method outperforms or at least remains competitive compared to these two SOTA methods. PatchAD attains superior results across multiple datasets and multiple metrics. Despite PatchAD’s relatively simple network structure, its performance remains competitive. Table 2 demonstrates that our approach outperforms previous methods on univariate dataset UCR. This shows that our method can also fetch state-of-the-art performance on univariate datasets.

Figure 1 depicts the average performance of PatchAD compared to various baselines across multiple datasets (WADI, SWAT, PSM, NIPS-TS-SWAN). PatchAD has demonstrated a remarkable improvement in the F1 score, with a notable increase of **50.5%**. Additionally, there has been a **7.8%** improvement in the Aff-F1 score and a commendable **10.0%** boost in the AUC.

Table 2: Results on UCR dataset.

Metric	Acc	P	R	F1
AnomalyTrans	99.49	60.41	100	73.08
DCdetector	99.51	61.62	100	74.05
PatchAD (Ours)	99.52	72.72	100	84.00

4.3 Unveiling the Mechanisms

PatchAD leverages Inter and Intra Mixers to learn detailed and generalized features respectively, as demonstrated in Figure 8. Utilizing multiple patch sizes, as explored in Appendix (Figures 8a &

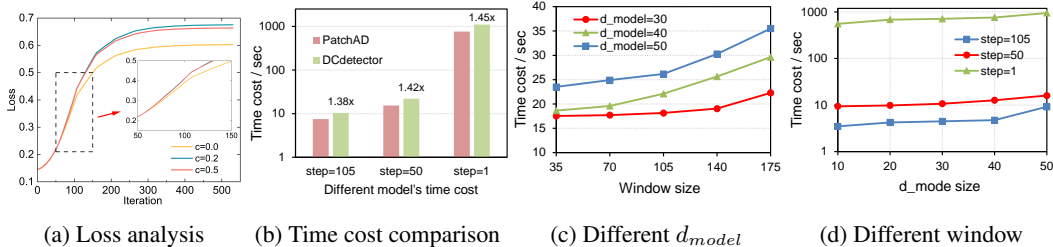


Figure 5: The analysis of PatchAD and DCdetector.

8b), enhances feature learning and generalization. The interplay between these mixers, visualized in Figure 3(c), effectively separates and amplifies distinct features, improving anomaly detection. Empirical validation, depicted in Figure 9, reveals that increasing patch size leads to more significant features acquired by the Intra Mixer, accelerating model learning. Finally, Figure 10 shows that anomalies are most easily detected in the Intra Mixer view due to its enhanced distinctiveness. In essence, maximizing the disparity between the Inter and Intra Mixers enhances PatchAD’s detection capabilities while mitigating overfitting. More details are provided in Appendix.

4.4 Model Analysis

4.4.1 Ablation Studies

To study the impact of different components in our model, we conducted ablation experiments across three datasets, as presented in Table 3. The ‘wo_ch_sharing’ method employs two independent Channel Mixer modules to model channel features, while ‘wo_ch_mixer’ denotes removing the Channel Mixer module. These two variants exhibit significant effects, particularly on the MSL and SMAP datasets, indicating that modelling inter-channel information and sharing channel information benefit model learning. Besides, ‘wo_pos_emb’ represents a variant without positional encoding, and removing positional encoding significantly affects PatchAD, highlighting the crucial role of positional encoding in its design. Furthermore, ‘wo_constraint’ showcases the impact of removing the constraint on the projection head. In conjunction with Figure 5a, we observed that a certain level of constraint facilitates easier model optimization, leading to improved results. This constraint prevents the model from converging to trivial solutions. In subsequent experiments, the default setting for the projection head constraint is 0.2.

Table 3: Ablation studies on MSL, SMAP, WADI datasets.

Dataset	MSL				SMAP				WADI				
	Methods	Acc	P	R	F1	Acc	P	R	F1	Acc	P	R	F1
wo_ch_sharing	98.78	91.93	96.90	94.35	98.84	93.50	97.75	95.58	98.71	84.99	94.25	89.38	
wo_ch_mixer	98.78	92.03	96.82	94.36	98.77	93.50	97.10	95.27	98.92	85.40	97.93	91.24	
wo_mixrep_mixer	96.41	89.54	74.66	81.43	95.25	91.52	68.55	78.70	95.76	67.55	51.99	58.76	
wo_pos_emb	97.85	91.51	87.73	89.58	96.47	92.18	79.13	85.16	98.23	83.96	85.53	84.74	
wo_constraint	98.51	91.67	94.49	93.06	99.01	93.55	99.05	96.22	98.73	85.26	94.25	89.53	
PatchAD (Ours)	98.92	92.05	98.20	95.02	99.10	94.45	98.75	96.55	99.06	85.92	100.00	92.43	

4.4.2 Parameter Sensitivity

A sensitivity analysis was conducted to investigate the impact of various PatchAD parameters on model performance (Figure 6). We find that a projection head constraint within the range of 0.1 to 0.4 is generally advisable, particularly for smaller datasets (Figure 6(a)). Optimal anomaly thresholds (σ) typically fall between 0.8 and 1.0, demonstrating robustness across various datasets (Figure 6(b)). A network dimension (d_{model}) of 40 strikes a balance between model complexity and performance (Figure 6(c)). PatchAD exhibits consistent performance across a range of window sizes (Figure 6(e)), and employing 3 or 4 encoder layers is found to be suitable (Figure 6(d)). Finally, combining multiple patch sizes demonstrates a positive impact on overall performance (Figure 6(f)). Detailed analysis for each parameter is provided in Appendix.

4.4.3 Visual Analysis

We visualized PatchAD’s response to various anomalies in Figure 4. Synthetic univariate time series were generated by [53], incorporating global point anomalies, contextual point anomalies, and pattern anomalies such as seasonal, group, and trend-based anomalies. The first row depicts the original data, while the second row displays PatchAD’s output of anomaly scores against the anomaly threshold.

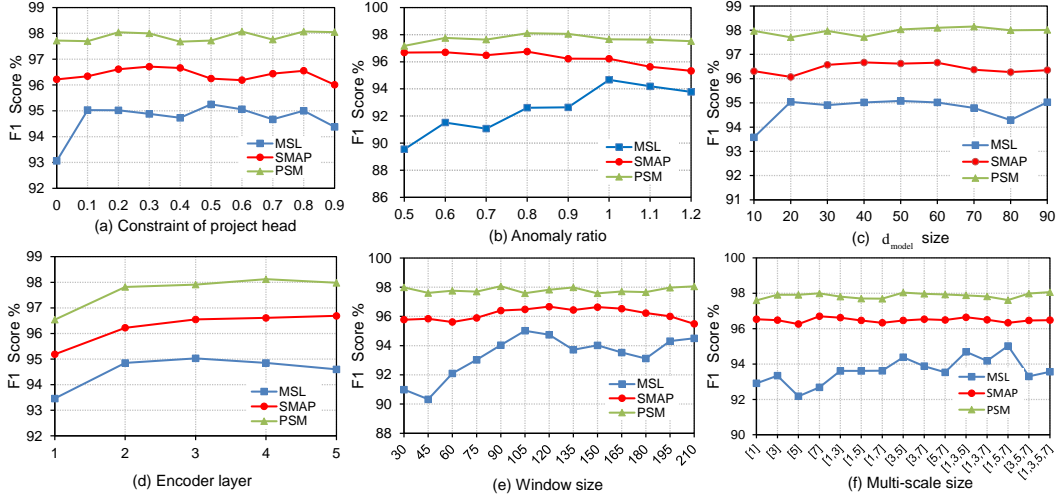


Figure 6: Parameter sensitivity studies of main hyper-parameters in PatchAD.

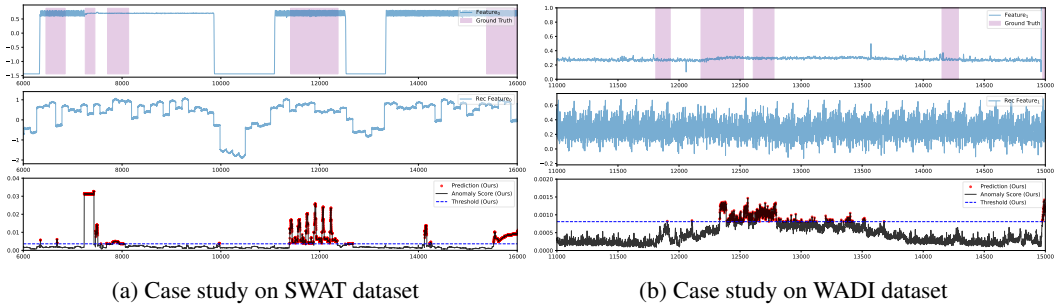


Figure 7: The case studies on SWAT and WADI datasets.

In particular, PatchAD has the ability to detect various types of anomalies. Figure 7 presents the practical performance of PatchAD on two real-world datasets. PatchAD exhibits the capability to detect the majority of anomalies, albeit with two anomalies remaining undetected. Furthermore, a noticeable disparity is observed between the reconstructed features by PatchAD and the original features, indicating its proficiency in learning the underlying patterns within the data, rather than simply replicating the original features.

4.4.4 Time Cost

We conducted a time consumption analysis on the SMD dataset under identical experimental conditions. Figure 5b demonstrates that under different sliding step conditions, our method outperforms DCdetector. Specifically, when the step is set to 1, PatchAD’s speed is 1.45x faster than DCdetector. Additionally, Figure 5d illustrates the time required for model training with a fixed window size (window size=105). This indicates that PatchAD exhibits higher efficiency in training compared to DCdetector. Figure 5c shows the time required for model training with a fixed sliding step (step=35) while varying the window size from 35 to 175 for different d_{model} sizes. Both graphs show that the time consumption of PatchAD exhibits a linear growth with respect to the independent variables. Thus, increasing the window size or enlarging d_{model} has a relatively minor impact on PatchAD. However, the time step noticeably affects the duration as this parameter increases data volume.

4.4.5 Model Size

Figure 2 compares the sizes of different models on SWAT dataset. Our model has a compact size of only 3.2MB, which is smaller than both AnomTrans and DCdetector, and significantly smaller than the LLM model (GPT2-Adapter) and diffusion model (D3R). This observation indicates that our model is more lightweight and resource-efficient.

5 Conclusion

We presents PatchAD, an innovative algorithm tailored for time series anomaly detection. PatchAD developed a lightweight multi-scale, patch-based MLP Mixer architecture grounded in contrastive learning. This architecture is unique in using a purely MLP-based approach to discern inter-patch and intra-patch relationships in time series sequences. By amplifying the differences between two data views, PatchAD enhance its capability to differentiate between normal and anomalous patterns. Furthermore, PatchAD adeptly learns the relationships between different data channels and incorporates a Dual Project Constraint to avert model degradation. Moreover, the efficacy of PatchAD, including its various components, is validated through extensive experimentation. The results demonstrate that proposed lightweight PatchAD outperforms over 30 methods across nine benchmark datasets from different application scenarios.

References

- [1] Mohammed Ayalew Belay, Sindre Stenen Blakseth, Adil Rasheed, and Pierluigi Salvo Rossi. Unsupervised Anomaly Detection for IoT-Based Multivariate Time Series: Existing Solutions, Performance Analysis and Future Directions. *Sensors*, 23(5):2844, 2023.
- [2] Kukjin Choi, Jihun Yi, Changhwa Park, and Sungroh Yoon. Deep Learning for Anomaly Detection in Time-Series Data: Review, Analysis, and Guidelines. *IEEE Access*, 9:120043–120065, 2021.
- [3] Zhijie Zhong, Kaixiang Yang, Zhiwen Yu, Yifan Shi, and C. L. Philip Chen. Towards efficient anomaly detection using memory broad learning system. In *2023 9th International Conference on Control Science and Systems Engineering (ICCSSE)*, pages 252–257, 2023.
- [4] Yiyuan Yang, Yi Li, Taojia Zhang, Yan Zhou, and Haifeng Zhang. Early safety warnings for long-distance pipelines: A distributed optical fiber sensor machine learning approach. In *Proceedings of the AAAI Conference on Artificial Intelligence*, volume 35, pages 14991–14999, 2021.
- [5] Yiyuan Yang, Haifeng Zhang, and Yi Li. Pipeline safety early warning by multifeature-fusion cnn and lightgbm analysis of signals from distributed optical fiber sensors. *IEEE Transactions on Instrumentation and Measurement*, 70:1–13, 2021.
- [6] Daehyung Park, Yuuna Hoshi, and Charles C Kemp. A multimodal anomaly detector for robot-assisted feeding using an lstm-based variational autoencoder. *IEEE Robotics and Automation Letters*, 3(3):1544–1551, 2018.
- [7] Ya Su, Youjian Zhao, Chenhao Niu, Rong Liu, Wei Sun, and Dan Pei. Robust anomaly detection for multivariate time series through stochastic recurrent neural network. In *Proceedings of the 25th ACM SIGKDD international conference on knowledge discovery & data mining*, pages 2828–2837, 2019.
- [8] Markus M Breunig, Hans-Peter Kriegel, Raymond T Ng, and Jörg Sander. Lof: identifying density-based local outliers. In *Proceedings of the 2000 ACM SIGMOD international conference on Management of data*, pages 93–104, 2000.
- [9] Bo Zong, Qi Song, Martin Renqiang Min, Wei Cheng, Cristian Lumezanu, Daeki Cho, and Haifeng Chen. Deep autoencoding gaussian mixture model for unsupervised anomaly detection. In *International conference on learning representations*, 2018.
- [10] Yiyuan Yang, Chaoli Zhang, Tian Zhou, Qingsong Wen, and Liang Sun. Dcdetector: Dual attention contrastive representation learning for time series anomaly detection. In *Proc. 29th ACM SIGKDD International Conference on Knowledge Discovery & Data Mining (KDD 2023)*, page 3033–3045, 2023.
- [11] Emadeldeen Eldele, Mohamed Ragab, Zhenghua Chen, Min Wu, Chee Keong Kwoh, Xiaoli Li, and Cuntai Guan. Time-Series Representation Learning via Temporal and Contextual Contrasting, 2021. arXiv:2106.14112 [cs].
- [12] Oliver D Anderson. Time-series. 2nd edn., 1976.
- [13] Loic Bontemps, Van Loi Cao, James McDermott, and Nhien-An Le-Khac. Collective anomaly detection based on long short-term memory recurrent neural networks. In *Future Data and*

- Security Engineering: Third International Conference, FDSE 2016, Can Tho City, Vietnam, November 23-25, 2016, Proceedings 3*, pages 141–152. Springer, 2016.
- [14] Haixu Wu, Tengge Hu, Yong Liu, Hang Zhou, Jianmin Wang, and Mingsheng Long. Timesnet: Temporal 2d-variation modeling for general time series analysis. In *The eleventh international conference on learning representations*, 2022.
 - [15] Tian Zhou, Peisong Niu, Xue Wang, Liang Sun, and Rong Jin. One Fits All: Power General Time Series Analysis by Pretrained LM. *Advances in Neural Information Processing Systems*, 36:43322–43355, 2023.
 - [16] Hao Zhou, Ke Yu, Xuan Zhang, Guanlin Wu, and Anis Yazidi. Contrastive autoencoder for anomaly detection in multivariate time series. *Information Sciences*, 610:266–280, 2022.
 - [17] Julien Audibert, Pietro Michiardi, Frédéric Guyard, Sébastien Marti, and Maria A. Zuluaga. USAD: UnSupervised Anomaly Detection on Multivariate Time Series. In *Proceedings of the 26th ACM SIGKDD International Conference on Knowledge Discovery & Data Mining*, pages 3395–3404, Virtual Event CA USA, 2020. ACM.
 - [18] Weiqi Zhang, Chen Zhang, and Fugee Tsung. GRELEN: Multivariate Time Series Anomaly Detection from the Perspective of Graph Relational Learning. In *Thirty-First International Joint Conference on Artificial Intelligence*, volume 3, pages 2390–2397, 2022.
 - [19] Bernhard Schölkopf, John C Platt, John Shawe-Taylor, Alex J Smola, and Robert C Williamson. Estimating the support of a high-dimensional distribution. *Neural computation*, 13(7):1443–1471, 2001.
 - [20] David MJ Tax and Robert PW Duin. Support vector data description. *Machine learning*, 54:45–66, 2004.
 - [21] Mohsin Munir, Shoaib Ahmed Siddiqui, Andreas Dengel, and Sheraz Ahmed. DeepAnT: A Deep Learning Approach for Unsupervised Anomaly Detection in Time Series. *IEEE Access*, 7:1991–2005, 2019.
 - [22] Jina Kim, Hyeongwon Kang, and Pilsung Kang. Time-series anomaly detection with stacked Transformer representations and 1D convolutional network. *Engineering Applications of Artificial Intelligence*, 120:105964, 2023.
 - [23] Zekai Chen, Dingshuo Chen, Xiao Zhang, Zixuan Yuan, and Xiuzhen Cheng. Learning Graph Structures with Transformer for Multivariate Time Series Anomaly Detection in IoT. *IEEE Internet of Things Journal*, 9(12):9179–9189, 2022. arXiv:2104.03466 [cs, eess].
 - [24] Hongzuo Xu, Yijie Wang, Songlei Jian, Qing Liao, Yongjun Wang, and Guansong Pang. Calibrated One-class Classification for Unsupervised Time Series Anomaly Detection, 2022.
 - [25] Chris U. Carmona, François-Xavier Aubet, Valentin Flunkert, and Jan Gasthaus. Neural contextual anomaly detection for time series, July 2021.
 - [26] Longyuan Li, Junchi Yan, Haiyang Wang, and Yaohui Jin. Anomaly Detection of Time Series With Smoothness-Inducing Sequential Variational Auto-Encoder. *IEEE Transactions on Neural Networks and Learning Systems*, 32(3):1177–1191, 2021. Conference Name: IEEE Transactions on Neural Networks and Learning Systems.
 - [27] Jiehui Xu, Haixu Wu, Jianmin Wang, and Mingsheng Long. Anomaly Transformer: Time Series Anomaly Detection with Association Discrepancy. 2021.
 - [28] Yiyuan Yang, Ming Jin, Haomin Wen, Chaoli Zhang, Yuxuan Liang, Lintao Ma, Yi Wang, Chenghao Liu, Bin Yang, Zenglin Xu, et al. A survey on diffusion models for time series and spatio-temporal data. *arXiv preprint arXiv:2404.18886*, 2024.
 - [29] Ilya O Tolstikhin, Neil Houlsby, Alexander Kolesnikov, Lucas Beyer, Xiaohua Zhai, Thomas Unterthiner, Jessica Yung, Andreas Steiner, Daniel Keysers, Jakob Uszkoreit, et al. Mlp-mixer: An all-mlp architecture for vision. *Advances in neural information processing systems*, 34:24261–24272, 2021.
 - [30] Si-An Chen, Chun-Liang Li, Nate Yoder, Sercan O Arik, and Tomas Pfister. Tsmixer: An all-mlp architecture for time series forecasting. *arXiv preprint arXiv:2303.06053*, 2023.
 - [31] Yuqi Nie, Nam H. Nguyen, Phanwadee Sinthong, and Jayant Kalagnanam. A Time Series is Worth 64 Words: Long-term Forecasting with Transformers, 2023.

- [32] Zeying Gong, Yujin Tang, and Junwei Liang. PatchMixer: A Patch-Mixing Architecture for Long-Term Time Series Forecasting, 2023.
- [33] Jean-Bastien Grill, Florian Strub, Florent Alché, Corentin Tallec, Pierre Richemond, Elena Buchatskaya, Carl Doersch, Bernardo Avila Pires, Zhaohan Guo, Mohammad Gheshlaghi Azar, et al. Bootstrap your own latent-a new approach to self-supervised learning. *Advances in neural information processing systems*, 33:21271–21284, 2020.
- [34] Xinlei Chen and Kaiming He. Exploring simple siamese representation learning. In *Proceedings of the IEEE/CVF conference on computer vision and pattern recognition*, pages 15750–15758, 2021.
- [35] Theivendiram Pranavan, Terence Sim, Arulmurugan Ambikapathi, and Savitha Ramasamy. Contrastive predictive coding for Anomaly Detection in Multi-variate Time Series Data, 2022.
- [36] Ting Chen, Simon Kornblith, Mohammad Norouzi, and Geoffrey Hinton. A simple framework for contrastive learning of visual representations. In *International conference on machine learning*, pages 1597–1607. PMLR, 2020.
- [37] Fei Tony Liu, Kai Ming Ting, and Zhi-Hua Zhou. Isolation forest. In *2008 eighth IEEE international conference on data mining*, pages 413–422. IEEE, 2008.
- [38] Mathias Perslev, Michael Jensen, Sune Darkner, Poul Jørgen Jennum, and Christian Igel. U-time: A fully convolutional network for time series segmentation applied to sleep staging. *Advances in Neural Information Processing Systems*, 32, 2019.
- [39] Youjin Shin, Sangyup Lee, Shahroz Tariq, Myeong Shin Lee, Okchul Jung, Daewon Chung, and Simon S Woo. Itad: integrative tensor-based anomaly detection system for reducing false positives of satellite systems. In *Proceedings of the 29th ACM international conference on information & knowledge management*, pages 2733–2740, 2020.
- [40] Takehisa Yairi, Naoya Takeishi, Tetsuo Oda, Yuta Nakajima, Naoki Nishimura, and Noboru Takata. A data-driven health monitoring method for satellite housekeeping data based on probabilistic clustering and dimensionality reduction. *IEEE Transactions on Aerospace and Electronic Systems*, 53(3):1384–1401, 2017.
- [41] Shahroz Tariq, Sangyup Lee, Youjin Shin, Myeong Shin Lee, Okchul Jung, Daewon Chung, and Simon S Woo. Detecting anomalies in space using multivariate convolutional lstm with mixtures of probabilistic pca. In *Proceedings of the 25th ACM SIGKDD international conference on knowledge discovery & data mining*, pages 2123–2133, 2019.
- [42] Shohreh Deldari, Daniel V Smith, Hao Xue, and Flora D Salim. Time series change point detection with self-supervised contrastive predictive coding. In *Proceedings of the Web Conference 2021*, pages 3124–3135, 2021.
- [43] Bin Zhou, Shenghua Liu, Bryan Hooi, Xueqi Cheng, and Jing Ye. Beatgan: Anomalous rhythm detection using adversarially generated time series. In *IJCAI*, volume 2019, pages 4433–4439, 2019.
- [44] Ryan Prescott Adams and David JC MacKay. Bayesian online changepoint detection. *arXiv preprint arXiv:0710.3742*, 2007.
- [45] Lukas Ruff, Robert Vandermeulen, Nico Goernitz, Lucas Deecke, Shoaib Ahmed Siddiqui, Alexander Binder, Emmanuel Müller, and Marius Kloft. Deep one-class classification. In *International conference on machine learning*, pages 4393–4402. PMLR, 2018.
- [46] Kyle Hundman, Valentino Constantinou, Christopher Laporte, Ian Colwell, and Tom Soderstrom. Detecting spacecraft anomalies using lstms and nonparametric dynamic thresholding. In *Proceedings of the 24th ACM SIGKDD international conference on knowledge discovery & data mining*, pages 387–395, 2018.
- [47] Zhihan Li, Youjian Zhao, Jiaqi Han, Ya Su, Rui Jiao, Xidao Wen, and Dan Pei. Multivariate time series anomaly detection and interpretation using hierarchical inter-metric and temporal embedding. In *Proceedings of the 27th ACM SIGKDD conference on knowledge discovery & data mining*, pages 3220–3230, 2021.
- [48] Lifeng Shen, Zhuocong Li, and James Kwok. Timeseries anomaly detection using temporal hierarchical one-class network. *Advances in Neural Information Processing Systems*, 33:13016–13026, 2020.

- [49] Yuqi Nie, Nam H Nguyen, Phanwadee Sinthong, and Jayant Kalagnanam. A time series is worth 64 words: Long-term forecasting with transformers. *arXiv preprint arXiv:2211.14730*, 2022.
- [50] Chih-Yu (Andrew) Lai, Fan-Keng Sun, Zhengqi Gao, Jeffrey H. Lang, and Duane Boning. Nominality Score Conditioned Time Series Anomaly Detection by Point/Sequential Reconstruction. *Advances in Neural Information Processing Systems*, 36:76637–76655, 2023.
- [51] Alexis Huet, Jose Manuel Navarro, and Dario Rossi. Local evaluation of time series anomaly detection algorithms. In *Proceedings of the 28th ACM SIGKDD Conference on Knowledge Discovery and Data Mining*, pages 635–645, 2022.
- [52] John Paparrizos, Paul Boniol, Themis Palpanas, Ruey S Tsay, Aaron Elmore, and Michael J Franklin. Volume under the surface: a new accuracy evaluation measure for time-series anomaly detection. *Proceedings of the VLDB Endowment*, 15(11):2774–2787, 2022.
- [53] Kwei-Herng Lai, Daochen Zha, Junjie Xu, Yue Zhao, Guanchu Wang, and Xia Hu. Revisiting time series outlier detection: Definitions and benchmarks. In *Thirty-fifth conference on neural information processing systems datasets and benchmarks track (round 1)*, 2021.
- [54] Wenke Lee and Dong Xiang. Information-theoretic measures for anomaly detection. In *Proceedings 2001 IEEE Symposium on Security and Privacy. S&P 2001*, pages 130–143. IEEE, 2000.
- [55] Mayu Sakurada and Takehisa Yairi. Anomaly detection using autoencoders with nonlinear dimensionality reduction. In *Proceedings of the MLSDA 2014 2nd workshop on machine learning for sensory data analysis*, pages 4–11, 2014.
- [56] Peter J Rousseeuw and Annick M Leroy. *Robust regression and outlier detection*. John wiley & sons, 2005.
- [57] Chin-Chia Michael Yeh, Yan Zhu, Liudmila Ulanova, Nurjahan Begum, Yifei Ding, Hoang Anh Dau, Diego Furtado Silva, Abdullah Mueen, and Eamonn Keogh. Matrix profile i: all pairs similarity joins for time series: a unifying view that includes motifs, discords and shapelets. In *2016 IEEE 16th international conference on data mining (ICDM)*, pages 1317–1322. IEEE, 2016.
- [58] Shereen Elsayed, Daniela Thyssens, Ahmed Rashed, Hadi Samer Jomaa, and Lars Schmidt-Thieme. Do we really need deep learning models for time series forecasting? *arXiv preprint arXiv:2101.02118*, 2021.
- [59] Shreshth Tuli, Giuliano Casale, and Nicholas R. Jennings. TranAD: Deep Transformer Networks for Anomaly Detection in Multivariate Time Series Data, 2022.
- [60] Chengsen Wang, Zirui Zhuang, Qi Qi, Jingyu Wang, Xingyu Wang, Haifeng Sun, and Jianxin Liao. Drift doesn't matter: Dynamic decomposition with diffusion reconstruction for unstable multivariate time series anomaly detection. *Advances in Neural Information Processing Systems*, 36, 2024.

Appendix

This is the appendix of PatchAD: A Lightweight Patch-Based MLP-Mixer for Time Series Anomaly Detection.

A Theory

In this section, our objective is to perform a theoretical analysis of PatchAD’s effectiveness. We want to prove that normal time series data points exhibit reduced information entropy. We have made the following assumptions based on the theoretical analysis presented in previous studies.

Assumption 1: The distribution of normal data differs from that of anomalies, and both consist of two components, denoted as $\tau + \alpha$. Here, τ represents the underlying data pattern, while α represents the pattern of normal or anomalous data. Therefore, we denote normal data distribution by Π and anomalies as Ω . As a result, the normal data \mathcal{X}_{norm} and the anomalous data \mathcal{X}_{anom} can be expressed as follows:

$$\mathcal{X}_{norm} = \tau + \pi, \text{ and } \mathcal{X}_{anom} = \tau + \omega. \quad (12)$$

Assumption 2: The number of normal data samples in the dataset is significantly larger than that of anomalous data samples. Therefore, we have the following relationship:

$$|\mathcal{X}_{norm}| = \zeta \cdot |\mathcal{X}_{anom}| > |\mathcal{X}_{anom}|, \quad (13)$$

where $|\cdot|$ represents the number of samples in the data, and ζ is a large number. We denote the entire dataset as $\mathcal{D} = \{\mathcal{X}_{norm}, \mathcal{X}_{anom}\}$.

Proof 1: The entropy of the anomalous data is higher than that of normal data. For a random variable X , its entropy is defined as, and the entropy serves as a metric for quantifying the uncertainty and complexity of the data [54]:

$$H(X) = - \sum_i p(x_i) \log_2 p(x_i) \quad (14)$$

According to Assumption 1, we have the representations of normal and anomalous data as follows: Normal data: $\mathcal{X}_{norm} = \tau + \pi$, where τ represents the underlying data pattern and π represents the data pattern of normal data. Anomalous data: $\mathcal{X}_{anom} = \tau + \omega$, where ω represents the data pattern of anomalous data. Based on Assumption 2, the number of samples in normal data ($|\mathcal{X}_{norm}|$) is much larger than the number of samples in anomalous data ($|\mathcal{X}_{anom}|$), given by $|\mathcal{X}_{norm}| = \zeta \cdot |\mathcal{X}_{anom}|$, where ζ is a large number. First, one calculates the entropy of the normal data $H(\mathcal{X}_{norm})$. According to the definition of entropy, we have: $H(\mathcal{X}_{norm}) = - \int p(\mathcal{X}_{norm}) \log p(\mathcal{X}_{norm}) d\mathcal{X}_{norm}$. Substituting $\mathcal{X}_{norm} = \tau + \pi$ into the above equation, we get: $H(\mathcal{X}_{norm}) = - \int p(\tau + \pi) \log p(\tau + \pi) d(\tau + \pi)$.

Using the addition rule of probability, we have $p(\tau + \pi) = p(\tau) \cdot p(\pi)$. Substituting this into the previous equation, we obtain: $H(\mathcal{X}_{norm}) = - \int p(\tau) \cdot p(\pi) \log(p(\tau) \cdot p(\pi)) d(\tau + \pi)$. Expanding further, we can deduce:

$$H(\mathcal{X}_{norm}) = - \int p(\tau) \cdot p(\pi) (\log p(\tau) + \log p(\pi)) d(\tau + \pi). \quad (15)$$

Since τ represents the underlying data pattern, we can separate the terms related to π in the first integral: $H(\mathcal{X}_{norm}) = - \int p(\tau) \log p(\tau) d\tau - \int p(\tau) \cdot p(\pi) \log p(\pi) d\pi$. The first integral is the entropy of the underlying data pattern $H(\tau)$. The second integral is the entropy of the normal data pattern $H(\pi)$. Therefore, we can further simplify the equation as: $H(\mathcal{X}_{norm}) = H(\tau) + H(\pi)$. Similarly, we can compute the entropy of the anomalous data $H(\mathcal{X}_{anom})$: $H(\mathcal{X}_{anom}) = H(\tau) + H(\omega)$.

Due to the significantly larger number of samples in normal data compared to anomalous data, i.e., $|\mathcal{X}_{norm}| = \zeta \cdot |\mathcal{X}_{anom}| > |\mathcal{X}_{anom}|$, we can extract the large number ζ and use the properties of logarithm to move it inside the log function:

$$H(\mathcal{X}_{norm}) = -\zeta \sum_{x \in \mathcal{X}_{norm}} P'(x) \log P'(x) - \zeta \sum_{x \in \mathcal{X}_{norm}} P'(x) \log \zeta \quad (16)$$

The second term $-\zeta \sum_{x \in \mathcal{X}_{norm}} P'(x) \log \zeta$ is a constant term, denoted as C .

Therefore, we can express the entropy of normal data as:

$$H(\mathcal{X}_{norm}) = -\zeta \sum_{x \in \mathcal{X}_{norm}} P'(x) \log P'(x) + C. \quad (17)$$

Similarly, we can derive the entropy of anomalous data $H(\mathcal{X}_{anom})$:

$$H(\mathcal{X}_{anom}) = - \sum_{x \in \mathcal{X}_{anom}} P'(x) \log P'(x). \quad (18)$$

At this point, we can conclude that $H(\pi) < H(\omega)$. Therefore, the entropy of normal data $H(\mathcal{X}_{norm})$ is smaller than the entropy of anomalous data $H(\mathcal{X}_{anom})$.

B Experimental Settings

B.1 Datasets

We applied eight multivariable and one univariable datasets for evaluation: (1) MSL (2) SMAP ⁴(3) PSM (4) SMD ⁵ (5) SWaT ⁶ (6) WADI ⁷ (7) NIPS-TS-SWAN (8) NIPSTS-GECCO ⁸. (9) UCR ⁹ Table 4 shows the details.

Table 4: Details of benchmark datasets.

Dataset	#Training	#Test (Labeled)	Dimension	Anomaly ratio (%)
MSL	58317	73729	55	10.5
SMAP	135183	427617	25	12.8
PSM	132481	87841	25	27.8
SMD	708377	708393	38	4.2
SWaT	99000	89984	26	12.2
WADI	1048571	172801	123	5.99
NIPS-TS-SWAN	60000	60000	38	32.6
NIPS-TS-GECCO	69260	69261	9	1.1

B.2 Baselines

We compared our model against 35 benchmark models, including: (1) Reconstruction-based: AutoEncoder [55], LSTM-VAE [6], OmniAnomaly [7], BeatGAN [43], InterFusion [47], USAD [17], COUTA[24]; (2) Autoregression-based: VAR [12], Autoregression [56], LSTM-RNN [13], LSTM [46], CL-MPPCA [41], TimesNet [14], NPSR-pt and NPSR-seq [50]; (3) Density-based: LOF [8], MMPCACD [40], DAGMM [9]; (4) Clustering-based: DeepSVDD [45], THOC [48], ITAD [39]; Matrix Profile [57]; (5) The classic methods: OCSVM [19], OCSVM-based subsequence clustering (OCSVM*), IForest [37], IForest-based subsequence clustering (IForest*), Gradient boosting regression (GBRT) [58]; (6) Change point detection and time series segmentation methods: BOCPD [44], U-Time [38], TS-CP2 [42]; (7) Transformer-based: Anomaly Transformer ¹⁰ [27], DCdetector ¹¹ [10], TranAD [59]; (8) Large Language Model: GPT2-Adapter[15]; (9) Diffusion model: D3R [60]; These two are current state-of-the-art methods.

B.3 Implementation Details

All experiments used PyTorch implementation on a single NVIDIA GTX 1080TI GPU. We summarize the default hyperparameters of PatchAD as follows: PatchAD consists of 3 encoder layers ($L=3$).

⁴MSL & SMAP: <https://github.com/ML4ITS/mtad-gat-pytorch>

⁵<https://github.com/NetManAI0ps/OmniAnomaly>

⁶https://itrust.sutd.edu.sg/itrust-labs_datasets

⁷<https://itrust.sutd.edu.sg/testbeds/water-distribution-wadi>

⁸Others:<http://github.com/DAMO-DI-ML/KDD2023-DCdetector>

⁹https://www.cs.ucr.edu/~eamonn/time_series_data_2018/UCR_TimeSeriesAnomalyDatasets2021.zip

¹⁰<https://github.com/thuml/Anomaly-Transformer>

¹¹<https://github.com/DAMO-DI-ML/KDD2023-DCdetector>

The hidden layer dimension d_{model} is set to 40. The default projector constraint coefficient is 0.2. The Adam optimizer’s default learning rate is 10^{-4} , with a batch size of 128, trained for 3 epochs across all datasets. Different patch sizes and window sizes were chosen for each dataset, defaulting to [3, 5] and 105, respectively. If an anomaly score of any given timestamp exceeds a threshold σ , the model identifies it as an anomaly. The default value for σ is 1.

C Algorithm’s Pseudo-code

Algorithm 1 PatchAD’s Python-like code

```

PE = PositionEmbedding(d_model) # Positional Embedding
VE_n, VE_p = Linear(dim1, d_model), Linear(dim2, d_model)
# Value Embedding of N and P views

# Patching and Embedding
x = PE(x)
x_n = rearrange(x, 'b (n p) c -> b c n p', p=patch_size)
x_p = rearrange(x, 'b (p n) c -> b c p n', p=patch_size)
x_n = VE_n(x_n)
x_p = VE_p(x_p)
# x_n's shape (B, c_dim, n_dim, d_model)
# x_p's shape (B, c_dim, p_dim, d_model)

Channel_Mixer = MLP(c_dim, transpose_dim=1)
Inter_Mixer = MLP(n_dim, transpose_dim=2)
Intra_Mixer = MLP(p_dim, transpose_dim=2)
MixRep_Mixer = MLP(d_model, transpose_dim=3)

# Patch Mixer Encoding
x_inter = Channel_Mixer(x_n)
x_intra = Channel_Mixer(x_p)
x_inter = Inter_Mixer(x_inter)
x_intra = Intra_Mixer(x_intra)
x_inter = MixRep_Mixer(x_inter)
x_intra = MixRep_Mixer(x_intra)

# Dual Project
x_inter = x_inter.mean(1)
x_intra = x_intra.mean(1)
Inter_Proj = MLP(d_model)
Intra_Proj = MLP(d_model)
x_inter2 = Inter_Proj(x_inter)
x_intra2 = Intra_Proj(x_intra)
# Output shape (B, n_dim, d_model) and (B, p_dim, d_model)
# Upsample to (B, L, d_model)

rec1 = Rec1(x_inter)
rec2 = Rec2(x_intra)
rec_x = rec1 + rec2

# Update
def loss_fn(a, b):
    return KL(a, b.detach()) + KL(b.detach(), a)

def inter_intra_loss_fn(n, p):
    return loss_fn(n, p) - loss_fn(p, n)

loss1 = inter_intra_loss_fn(x_inter, x_intra)

loss_n_proj = inter_intra_loss_fn(x_inter, x_intra2)
loss_p_proj = inter_intra_loss_fn(x_intra2, x_intra)
loss_proj = loss_n_proj + loss_p_proj
loss_rec = MSE(rec_x, x)

final_loss = (1-c) * loss1 + c * loss_proj + loss_rec
# backward and optimize

```

D Unveiling the Mechanisms

Figure 8 illustrates the knowledge acquired by PatchAD in four distinct cases. Cases 2, 3, 4 and 5 have a patch size of 1, whereas case 1 has a patch size of [1, 2, 5]. The "**Original**" represents the original data, while "**Rec 1**" and "**Rec 2**" correspond to the features learned by the Inter Mixer and the Intra Mixer, respectively. It is observed that the Intra Mixer captures the generalized knowledge in the data, which encompasses the overall trend information. Conversely, the Inter Mixer learns the detailed features of the data, compensating for any aspects that may not be captured by the Intra Mixer. A comparison between case 1 and case 2 reveals that using three distinct patch scales facilitates the

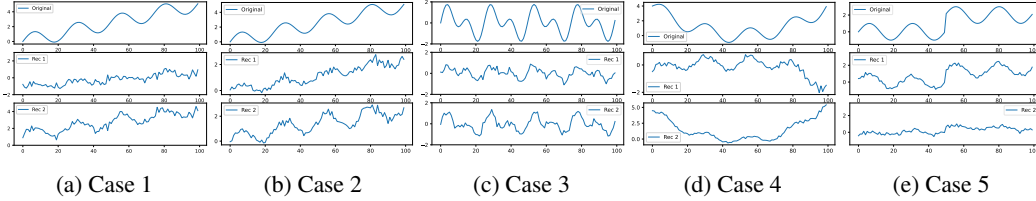


Figure 8: Visualization of the features learnt by Inter and Intra Mixer.

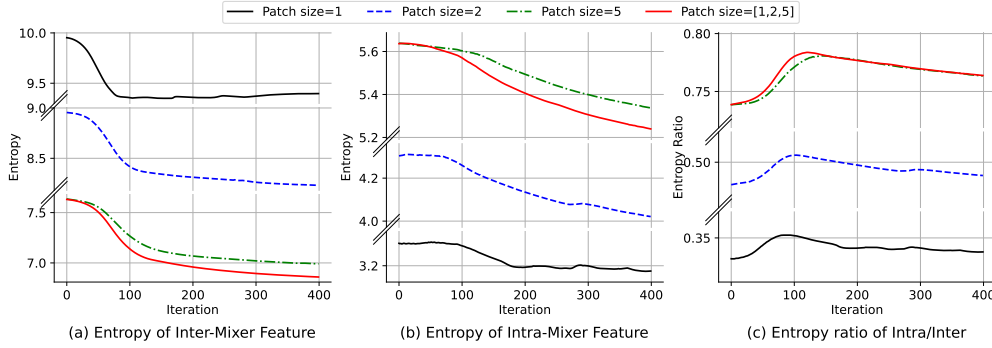


Figure 9: Entropy analysis.

acquisition of more detailed representations and enhances the generalization of the acquired features. Note that the y-axis ranges for Figure 8a and Figure 8b are different. Moreover, these two mixers collaborate to segregate and amplify the distinctive features effectively. The decoupling of features assists PatchAD in amplifying the anomaly-related characteristics, as indicated in Figure 3(c), thereby enhancing the detectability of anomalies. The superior performance of PatchAD can also be attributed to the varying sizes of the Inter and Intra Mixer branches, which prevent overfitting. This is the reason why PatchAD does not require the construction of negative samples in contrastive learning, as the two different networks construct implicit positive and negative samples.

Moreover, we empirically validate this conclusion through experiments. Case 1 was chosen as the baseline, and we investigated the entropy of the features acquired by the Inter and Intra Mixers under varying patch size conditions. Figures 9(a) and 9(b) illustrate that both the Inter Mixer and Intra Mixer display a consistent trend of decreasing entropy throughout the learning process. This observation suggests that the models effectively acquire knowledge and reduce uncertainty. Furthermore, we noticed that the Inter Mixer demonstrates the highest learning speed and exhibits the most substantial decrease in entropy when the patch size is configured as [1, 2, 5]. Additionally, as the patch size decreases, the entropy of the Inter Mixer increases, and it actually rises when the patch size is set to 1. This implies that the network is required to learn an excessive number of features. Figure 9(c) computes the ratio of Intra to Inter entropy, and our findings indicate that as the patch size increases, the features acquired by the Intra Mixer gain greater significance, thereby accelerating model learning through the utilization of multi-scale patch sizes.

Figure 10 illustrates the visualization of feature distributions in the SWAT dataset under three conditions. It is observed that anomalies are more easily detected in the Intra Mixer view (See Figure 10(b)), as its distinctiveness is more pronounced compared to the other two views (Figure 10(a) & (c)).

According to our analysis, maximizing the disparities between the Inter Mixer and Intra Mixer can enhance the model’s detection capabilities. During network optimization, the Inter-Intra loss compels the Intra Mixer to acquire more generalized representations, effectively mitigating model overfitting.

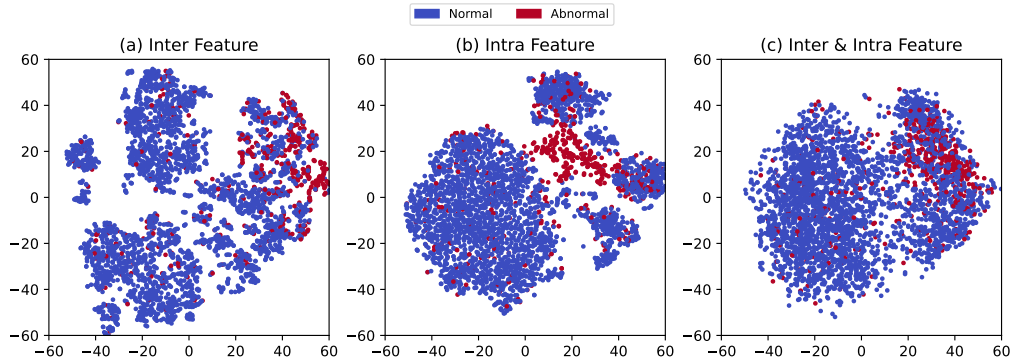


Figure 10: Latent distribution’s visualization by T-SNE.

E Parameter Sensitivity

We conducted a sensitivity analysis on PatchAD’s parameters. The default parameter settings remain consistent with the basic configuration. Figure 6(a) demonstrates the impact of the projection head constraint on PatchAD. Overall, it holds more significance for smaller-scale datasets like MSL. However, excessively strong constraints hinder the model’s learning process. Therefore, setting this constraint between 0.1 to 0.4 is more advisable. Figure 6(b) analyzes PatchAD’s final model performance when the anomaly threshold σ ranges from 0.5 to 1.2. The selection of the anomaly threshold appears more robust on the PSM and SMAP datasets than the MSL dataset. Setting this value between 0.8 and 1 for most datasets yields optimal results. Figure 6(c) illustrates how the model’s performance is influenced by the network dimension d_{model} . PatchAD demonstrates better results with smaller d_{model} sizes. Therefore, to balance model performance and complexity, we set $d_{model} = 40$ to ensure PatchAD operates effectively. Figure 6(d) indicates that PatchAD’s performance is influenced by the number of encoder layers, and given a compromise, we set it to 3 or 4. Figure 6(e) demonstrates PatchAD’s robustness concerning the window size, which ranges from 60 to 210. The time window is a critical parameter, typically set to an initial value of 105 across most datasets. Lastly, Figure 6(f) displays PatchAD’s performance under different multi-scale patch size combinations. (e.g., a patch size of [3,5] represents using two scales in PatchAD.) The outcomes suggest that combining various patch sizes can enhance PatchAD’s performance.

F Visualization comparison

Figure 11 shows the performance of WindowAD algorithms in the face of different types of anomalies. These methods have difficulty in detecting contextual and group point anomalies and are able to detect seasonal anomalies, but there are some false positives, which indicates that it has a low precision.

G Full Comparison Results

Table 6 presents the performance of different methods on four datasets, namely WADI, SWAT, PSM, and SWAN. This is the original data of Figure 1. We have selected representative algorithms for experimental comparison.

In Table 7, Aff-P and Aff-R are the precision and recall of affiliation metric [51], respectively. R_A_R and R_A_P are Range-AUC-ROC and Range-AUC-PR [52], respectively. V_ROC and V_RR are volumes under the surfaces created based on ROC curve and PR curve [52], respectively. Besides, we give more results in table 8, and the results from more real-world multivariate time-series datasets show that our proposed PatchAD has good robustness and performance.

H Limitations

Although PatchAD achieves optimal results on multiple datasets, some limitations still need to be addressed. In order to ensure the optimization of different metrics, subtle adjustments to potential

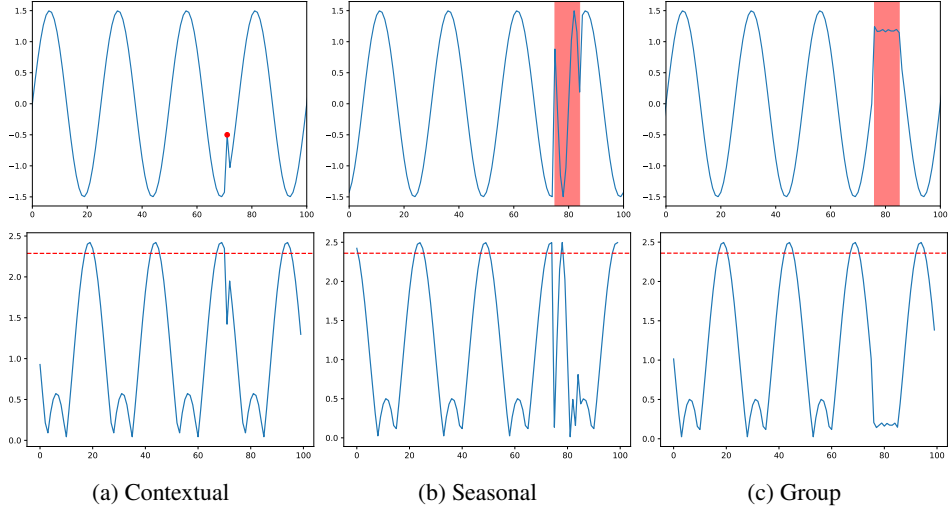


Figure 11: Visualization of WindowAD-based algorithm’s score.

Table 5: Overall results on NIPS-TS datasets. All results are in %, the best in **Bold**, and the second in underlined.

Dataset	NIPS-TS-SWAN			NIPS-TS-GECCO			Average F1
	P	R	F1	P	R	F1	
MatrixProfile [57]	16.70	17.50	17.10	4.60	18.50	7.40	12.25
GBRT [58]	44.70	37.50	40.80	17.50	14.00	15.60	28.20
LSTM-RNN [13]	52.70	22.10	31.20	34.30	27.50	30.50	30.85
Autoregression [56]	42.10	35.40	38.50	39.20	31.40	34.90	36.70
OCSVM [19]	47.40	49.80	48.50	18.50	74.30	29.60	39.05
IForest* [37]	40.60	42.50	41.60	39.20	31.50	39.00	40.30
AutoEncoder [55]	49.70	52.20	50.90	42.40	34.00	37.70	44.30
AnomalyTrans [27]	90.70	47.40	62.30	25.70	28.50	27.00	44.65
IForest [37]	56.90	59.80	58.30	43.90	35.30	39.10	48.70
AnomalyTrans [27]	90.71	47.43	62.29	29.96	48.63	37.08	49.69
DCdetector [10]	<u>96.57</u>	<u>59.08</u>	<u>73.31</u>	<u>38.41</u>	<u>59.73</u>	<u>46.76</u>	60.04
PatchAD (Ours)	96.75	59.15	73.41	40.62	62.88	49.35	61.38

parameters are necessary. For instance, selecting an appropriate anomaly threshold is crucial to balance precision and recall. Developing an automated threshold adjustment scheme is a potential avenue for future research. Time series anomaly detection employs a wide range of evaluation metrics, each with its own emphasis, leading to potential biases in evaluating different algorithms. In the future, we aim to propose a unified set of evaluation metrics that consider multiple factors, contributing to the advancement of the community.

I Broader Impacts

Time series anomaly detection has significant academic implications and broader impacts in various domains. In finance, it aids in detecting fraudulent activities like credit card fraud and insider trading, safeguarding financial systems and preventing losses. In healthcare, it aids in early disease detection and monitoring, enabling timely interventions and improved patient outcomes. Overall, time series anomaly detection improves decision-making, risk mitigation, and system performance across multiple domains.

Table 6: The performance of algorithms on different evaluation metrics without point adjustment.

Dataset	WADI							SWAT						
Metric	P	R	F1_ori	Aff-Pre	AFF-Rec	Aff-F1	AUC	P	R	F1_ori	Aff-Pre	AFF-Rec	Aff-F1	AUC
Deep SVDD	4.05	38.53	7.34	50.06	55.79	52.77	40.53	12.74	98.50	22.57	53.58	99.99	69.77	86.81
USAD	5.74	100.00	10.86	54.92	100.00	70.90	46.39	12.17	100.00	21.70	53.00	100.00	69.28	88.66
COUTA	98.72	15.58	<u>26.92</u>	99.18	23.08	37.44	49.48	94.25	6.33	11.87	79.98	33.20	46.92	75.54
TranAD	6.49	63.89	11.78	55.91	91.96	69.54	52.60	14.70	96.40	<u>25.50</u>	55.65	99.66	71.42	88.90
TimesNet	64.04	10.24	17.65	65.25	39.30	49.05	65.08	11.05	3.21	4.98	57.84	93.77	<u>71.55</u>	26.76
AnomTrans	4.14	14.12	6.40	45.73	40.66	43.05	49.20	4.81	29.32	8.27	53.03	98.08	36.08	19.20
DCdetector	5.80	14.42	8.27	59.63	90.98	69.98	49.88	15.49	5.54	8.16	52.76	97.33	68.94	50.68
GPT2-Adapter	5.68	5.50	5.59	55.62	98.29	71.04	50.01	12.16	0.96	1.78	52.51	98.13	68.41	50.00
D3R	6.99	80.99	12.86	56.47	99.98	72.17	51.39	32.87	75.97	45.89	61.47	78.52	68.96	79.95
PatchAD (Ours)	89.48(2.08)	31.22(0.74)	46.28(1.09)	73.07(0.41)	86.07(0.28)	79.04(0.12)	79.89(0.55)	85.42(0.98)	70.34(0.18)	77.15(0.48)	73.62(0.52)	84.65(0.22)	78.75(0.20)	91.19(0.12)
Dataset	PSM							SWAN						
Metric	P	R	F1_ori	Aff-Pre	AFF-Rec	Aff-F1	AUC	P	R	F1_ori	Aff-Pre	AFF-Rec	Aff-F1	AUC
Deep SVDD	28.59	99.91	44.46	53.92	99.98	70.06	78.09	41.74	85.03	55.99	56.84	89.93	69.66	75.32
USAD	32.36	92.17	47.90	55.30	98.71	70.88	64.53	39.73	77.94	52.63	55.26	68.62	61.22	66.76
COUTA	100.00	0.04	<u>0.08</u>	100.00	5.12	9.75	72.45	62.96	0.09	0.17	69.25	0.10	0.19	71.38
TranAD	35.90	54.23	43.20	60.88	92.09	73.30	65.22	38.84	78.29	51.93	57.86	90.18	70.49	70.00
TimesNet	64.85	1.27	2.49	77.84	67.23	72.15	58.74	38.63	48.89	43.16	60.75	81.29	69.53	53.62
AnomTrans	26.05	84.32	39.81	55.55	80.28	50.09	52.18	31.19	79.87	44.86	58.45	9.49	0.54	45.38
DCdetector	27.05	19.59	22.72	52.33	76.95	65.88	49.62	32.45	98.62	48.83	38.73	3.13	7.50	50.35
GPT2-Adapter	28.31	46.64	35.24	54.33	95.16	69.17	50.74	40.00	52.05	45.23	61.17	69.55	65.09	58.77
D3R	28.96	93.65	44.24	53.84	100.00	69.99	60.64	36.12	78.38	49.45	57.70	96.06	72.10	62.54
PatchAD (Ours)	47.13(0.44)	49.32(0.97)	48.20(0.64)	63.52(0.82)	96.84(1.21)	76.72(0.19)	64.74(0.01)	51.76(0.18)	65.31(0.47)	57.75(0.08)	66.48(0.80)	79.39(1.54)	72.36(0.20)	72.91(0.02)

Table 7: Multi-metrics results on all real-world multivariate datasets. All results are in %, the best in **Bold**, and the second in underlined.

Dataset	Method	Acc	F1	Aff-P	Aff-R	R_A_R	R_A_P	V_ROC	V_PR
MSL	AnomalyTrans	98.69	93.93	51.76	95.98	90.04	87.87	88.20	86.26
	DCdetector	<u>98.83</u>	<u>94.77</u>	51.01	96.74	91.29	89.12	<u>89.80</u>	<u>87.81</u>
	PatchAD	98.92	95.02	52.06	<u>96.44</u>	<u>90.89</u>	<u>88.66</u>	90.09	87.99
SMAP	AnomalyTrans	99.05	96.41	51.39	98.68	96.32	<u>94.07</u>	95.52	<u>93.37</u>
	DCdetector	<u>99.06</u>	<u>96.38</u>	50.29	98.04	93.76	92.40	92.70	91.47
	PatchAD	99.15	96.75	52.30	98.70	<u>96.05</u>	94.23	<u>95.12</u>	93.42
PSM	AnomalyTrans	98.68	97.37	55.35	80.28	91.83	93.03	88.71	90.71
	DCdetector	98.81	<u>97.63</u>	52.33	76.95	89.91	91.74	85.57	88.52
	PatchAD	98.95	98.11	55.58	82.72	94.85	95.65	89.26	91.67
SMD	AnomalyTrans	99.11	90.06	72.63	98.27	82.12	75.90	81.86	75.69
	DCdetector	98.78	86.02	51.61	93.44	76.13	69.85	73.60	67.45
	PatchAD	98.84	<u>86.62</u>	50.81	<u>93.32</u>	<u>77.55</u>	<u>71.16</u>	<u>74.09</u>	<u>67.88</u>
SWaT	AnomalyTrans	<u>98.62</u>	94.62	53.03	98.08	97.89	93.47	97.92	93.49
	DCdetector	93.25	<u>96.51</u>	52.76	97.33	98.23	<u>95.54</u>	<u>98.25</u>	<u>95.56</u>
	PatchAD	99.12	96.52	<u>52.78</u>	98.17	98.23	95.55	98.26	95.57
WADI	AnomalyTrans	98.17	85.47	87.84	99.75	87.20	78.50	<u>87.36</u>	78.63
	DCdetector	98.70	<u>89.26</u>	59.63	90.98	87.56	81.62	<u>87.16</u>	81.23
	PatchAD	99.06	92.43	<u>60.37</u>	<u>91.76</u>	89.85	84.18	90.68	84.99
NIPS-TS-SWAN	AnomalyTrans	84.57	62.29	58.45	9.49	86.42	93.26	84.81	92.00
	DCdetector	85.99	73.31	38.73	3.13	88.02	94.78	<u>86.02</u>	93.49
	PatchAD	86.05	73.41	<u>51.44</u>	4.34	88.03	94.80	86.13	93.57
NIPS-TS-GECCO	AnomalyTrans	98.26	37.08	55.65	<u>89.12</u>	60.74	28.17	60.48	28.02
	DCdetector	98.57	46.76	49.66	87.68	61.01	32.13	60.77	31.90
	PatchAD	98.64	49.35	<u>53.04</u>	89.48	63.59	35.92	63.09	35.43

Table 8: More results on all real-world multivariate datasets. All results are in %, the best in **Bold**, and the second in underlined.

Dataset	MSL			SMAP			PSM			SMD			SWaT			Average F1
	P	R	F1	P	R	F1	P	R	F1	P	R	F1	P	R	F1	
LOF	47.72	85.25	61.18	58.93	56.33	57.60	57.89	90.49	70.61	56.34	39.86	46.68	72.15	65.43	68.62	60.94
OCSVM	59.78	86.87	70.82	53.85	59.07	56.34	62.75	80.89	70.67	44.34	76.72	56.19	45.39	49.22	47.23	60.25
U-Time	57.20	71.66	63.62	49.71	56.18	52.75	82.85	79.34	81.06	65.95	74.75	70.07	46.20	87.94	60.58	65.62
IForest	53.94	86.54	66.45	52.39	59.07	55.53	76.09	92.45	83.48	42.31	73.29	53.64	49.29	44.95	47.02	61.22
DAGMM	89.60	63.93	74.62	86.45	56.73	68.51	93.49	70.03	80.08	67.30	49.89	57.30	89.92	57.84	70.40	70.18
ITAD	69.44	84.09	76.07	82.42	66.89	73.85	72.80	64.02	68.13	86.22	73.71	79.48	63.13	52.08	57.08	70.92
VAR	74.68	81.42	77.90	81.38	53.88	64.83	90.71	83.82	87.13	78.35	70.26	74.08	81.59	60.29	69.34	74.66
MMPCCAD	81.42	61.31	69.95	88.61	75.84	81.73	76.26	78.35	77.29	71.20	79.28	75.02	82.52	68.29	74.73	75.74
CL-MPPCA	73.71	88.54	80.44	86.13	63.16	72.88	56.02	99.93	71.80	82.36	76.07	79.09	76.78	81.50	79.07	76.66
TS-CP2	86.45	68.48	76.42	87.65	83.18	85.36	82.67	78.16	80.35	87.42	66.25	75.38	81.23	74.10	77.50	79.00
Deep-SVDD	91.92	76.63	83.58	89.93	56.02	69.04	95.41	86.49	90.73	78.54	79.67	79.10	80.42	84.45	82.39	80.97
BOCPD	80.32	87.20	83.62	84.65	85.85	85.24	80.22	75.33	77.70	70.90	82.04	76.07	89.46	70.75	79.01	80.33
LSTM-VAE	85.49	79.94	82.62	92.20	67.75	78.10	73.62	89.92	80.96	75.76	90.08	82.30	76.00	89.50	82.20	81.24
BeatGAN	89.75	85.42	87.53	92.38	55.85	69.61	90.30	93.84	92.04	72.90	84.09	78.10	64.01	87.46	73.92	80.24
LSTM	85.45	82.50	83.95	89.41	78.13	83.39	76.93	89.64	82.80	78.55	85.28	81.78	86.15	83.27	84.69	83.32
OmniAnomaly	89.02	86.37	87.67	92.49	81.99	86.92	88.39	74.46	80.83	83.68	86.82	85.22	81.42	84.30	82.83	84.69
InterFusion	81.28	92.70	86.62	89.77	88.52	89.14	83.61	83.45	83.52	<u>87.02</u>	85.43	86.22	80.59	85.58	83.01	85.70
THOC	88.45	90.97	89.69	92.06	89.34	90.68	88.14	90.99	89.54	79.76	<u>90.95</u>	84.99	83.94	86.36	85.13	88.01
AnomalyTrans	91.92	96.03	93.93	93.59	99.41	<u>96.41</u>	96.94	97.81	97.37	84.14	96.88	90.06	89.79	100.0	94.62	<u>94.48</u>
DCdetector	92.22	<u>97.48</u>	<u>94.77</u>	<u>94.43</u>	<u>98.41</u>	<u>96.38</u>	<u>97.19</u>	<u>98.08</u>	<u>97.63</u>	83.04	89.22	86.02	<u>93.25</u>	<u>100.0</u>	<u>96.51</u>	94.26
PatchAD	<u>92.05</u>	98.20	95.02	94.49	99.13	96.75	97.72	98.52	98.11	83.06	90.51	<u>86.62</u>	93.28	100.0	96.52	94.60

Table 9: Parameter studies on project head constraint results (patch size=[3,5], window size=105). All results are in %.

Dataset	MSL				SMAP				PSM			
	Constraint	Acc	P	R	F1	Acc	P	R	F1	Acc	P	R
0.0	98.51	91.67	94.49	93.06	99.01	93.55	99.05	96.22	98.73	97.42	98.03	97.72
0.1	98.92	91.96	98.33	95.03	99.04	94.43	98.33	96.34	98.72	97.35	98.04	97.70
0.2	98.92	92.05	98.20	95.02	99.11	94.42	98.91	96.61	98.91	97.43	98.66	98.04
0.3	98.89	92.03	97.93	94.88	99.14	94.41	99.11	96.71	98.89	97.42	98.59	98.00
0.4	98.86	92.09	97.54	94.73	99.12	94.45	98.97	96.66	98.71	97.42	97.94	97.68
0.5	98.96	92.12	98.60	95.25	99.02	94.40	98.17	96.25	98.73	97.42	98.03	97.72
0.6	98.92	92.11	98.20	95.06	99.01	94.39	98.07	96.19	98.92	97.45	98.70	98.07
0.7	98.84	91.91	97.59	94.67	99.07	94.43	98.55	96.44	98.76	97.39	98.14	97.76
0.8	98.91	92.01	98.20	95.00	99.10	94.40	98.81	96.55	98.92	97.42	98.73	98.07
0.9	98.78	91.99	96.90	94.38	98.96	94.37	97.70	96.01	98.92	97.47	98.64	98.05

Table 10: Parameter studies on anomaly threshold σ results (patch size=[3,5], window size=105). All results are in %.

Dataset	MSL				SMAP				PSM			
	AR	Acc	P	R	F1	Acc	P	R	F1	Acc	P	R
0.5	97.93	95.39	84.39	89.55	99.15	96.46	96.91	96.68	98.45	98.61	95.77	97.17
0.6	98.27	94.70	88.54	91.52	99.15	95.84	97.58	96.70	98.77	98.33	97.20	97.76
0.7	98.17	93.76	88.54	91.07	99.09	95.22	97.77	96.48	98.70	98.07	97.20	97.64
0.8	98.45	93.19	92.04	92.61	99.15	94.73	98.86	96.75	98.95	97.94	98.29	98.11
0.9	98.45	92.36	92.93	92.64	99.01	94.07	98.49	96.23	98.92	97.68	98.45	98.06
1.0	98.84	91.80	97.73	94.67	99.01	94.05	98.49	96.22	98.70	97.30	98.03	97.66
1.1	98.73	91.22	97.36	94.19	98.85	92.76	98.69	95.63	98.68	97.06	98.20	97.63
1.2	98.64	90.45	97.36	93.78	98.76	92.19	98.69	95.33	98.62	96.85	98.20	97.52

Table 11: Parameter studies on d_{model} size results (patch size=[3,5], window size=105). All results are in %.

d_{model}	MSL				SMAP				PSM			
	Acc	P	R	F1	Acc	P	R	F1	Acc	P	R	F1
10	98.62	91.81	95.42	93.58	99.04	94.42	98.28	96.31	98.87	97.38	98.56	97.97
20	98.92	92.08	98.20	95.04	98.98	94.33	97.88	96.07	98.73	97.37	98.05	97.71
30	98.89	92.06	97.94	94.91	99.10	94.43	98.80	96.57	98.87	97.43	98.52	97.97
40	98.91	92.03	98.20	95.02	99.13	94.49	98.95	96.67	98.73	97.42	98.03	97.72
50	98.93	92.15	98.20	95.08	99.11	94.45	98.89	96.62	98.90	97.44	98.63	98.03
60	98.91	92.03	98.20	95.02	99.13	94.44	98.98	96.66	98.94	97.48	98.74	98.10
70	98.87	92.08	97.67	94.79	99.05	94.40	98.43	96.37	98.97	97.48	98.83	98.15
80	98.77	91.99	96.70	94.29	99.03	94.38	98.24	96.27	98.89	97.44	98.58	98.00
90	98.92	92.06	98.20	95.03	99.05	94.38	98.42	96.35	98.89	97.46	98.56	98.01

Table 12: Parameter studies on encoder layers L results (patch size=[3,5], window size=105). All results are in %.

Encoder layer	MSL				SMAP				PSM			
	Acc	P	R	F1	Acc	P	R	F1	Acc	P	R	F1
1	98.60	91.72	95.27	93.46	98.76	94.29	96.11	95.19	98.10	97.28	95.82	96.54
2	98.88	91.96	97.93	94.85	99.01	94.42	98.09	96.22	98.79	97.44	98.20	97.82
3	98.92	92.07	98.20	95.03	99.10	94.41	98.79	96.55	98.84	97.47	98.36	97.91
4	98.88	92.19	97.67	94.85	99.11	94.42	98.91	96.61	98.95	97.41	98.83	98.12
5	98.83	91.95	97.41	94.60	99.13	94.46	99.02	96.69	98.87	97.44	98.52	97.98

Table 13: Parameter studies on window size results (window size=105). All results are in %.

Window size	MSL				SMAP				PSM			
	Acc	P	R	F1	Acc	P	R	F1	Acc	P	R	F1
30	98.11	91.47	90.52	90.99	98.91	94.38	97.23	95.78	98.88	97.48	98.51	97.99
45	97.98	91.23	89.44	90.33	98.93	95.55	96.14	95.84	98.67	97.30	97.92	97.61
60	98.33	92.05	92.16	92.10	98.86	94.18	97.09	95.62	98.75	97.59	97.93	97.76
75	98.51	91.79	94.31	93.03	98.93	94.27	97.60	95.90	98.72	97.35	98.06	97.70
90	98.71	91.92	96.24	94.03	99.06	94.34	98.55	96.40	98.92	97.44	98.71	98.07
105	98.92	92.05	98.20	95.02	99.08	94.44	98.60	96.48	98.66	97.38	97.79	97.59
120	98.86	92.10	97.55	94.75	99.13	94.47	98.98	96.67	98.79	97.53	98.13	97.83
135	98.65	91.85	95.67	93.72	99.07	94.46	98.50	96.44	98.88	97.38	98.60	97.99
150	98.71	91.83	96.30	94.02	99.12	94.48	98.91	96.64	98.66	97.43	97.72	97.58
165	98.61	91.85	95.27	93.53	99.09	94.50	98.65	96.53	98.73	97.44	97.98	97.71
180	98.53	91.73	94.55	93.12	99.01	94.35	98.18	96.23	98.70	97.55	97.78	97.66
195	98.77	92.02	96.70	94.31	98.96	94.35	97.74	96.01	98.87	97.44	98.50	97.97
210	98.81	91.97	97.17	94.50	98.83	94.30	96.71	95.49	98.92	97.45	98.69	98.06

Table 14: Parameter studies on multi-scale patch size results (window size=105). All results are in %.

Patch size	MSL				SMAP				PSM			
	Acc	P	R	F1	Acc	P	R	F1	Acc	P	R	F1
[1]	98.49	91.73	94.12	92.91	99.09	94.47	98.69	96.53	98.66	97.21	97.99	97.60
[3]	98.57	91.67	95.08	93.34	99.08	94.44	98.61	96.48	98.84	97.56	98.26	97.91
[5]	98.34	91.70	92.66	92.18	99.02	94.40	98.20	96.26	98.83	97.44	98.37	97.91
[7]	98.45	91.96	93.41	92.68	99.13	94.46	99.04	96.70	98.88	97.43	98.56	97.99
[1, 3]	98.63	91.87	95.42	93.61	99.11	94.48	98.86	96.62	98.78	97.46	98.16	97.81
[1, 5]	98.63	91.88	95.42	93.61	99.07	94.43	98.58	96.46	98.72	97.37	98.04	97.70
[1, 7]	98.63	91.89	95.42	93.62	99.04	94.43	98.32	96.33	98.71	97.39	97.99	97.69
[3, 5]	98.78	91.99	96.90	94.38	99.07	94.39	98.63	96.46	98.91	97.43	98.66	98.04
[3, 7]	98.68	91.92	95.93	93.88	99.09	94.40	98.76	96.53	98.87	97.41	98.55	97.97
[5, 7]	98.61	91.86	95.27	93.53	99.08	94.44	98.63	96.49	98.85	97.40	98.46	97.93
[1, 3, 5]	98.85	92.01	97.54	94.69	99.12	94.47	98.92	96.64	98.82	97.37	98.39	97.88
[1, 3, 7]	98.74	92.00	96.46	94.18	99.09	94.40	98.71	96.50	98.79	97.43	98.21	97.82
[1, 5, 7]	98.92	92.05	98.20	95.02	99.04	94.38	98.36	96.33	98.67	97.36	97.87	97.61
[3, 5, 7]	98.56	91.76	94.89	93.30	99.08	94.42	98.61	96.46	98.87	97.45	98.52	97.98
[1, 3, 5, 7]	98.62	91.78	95.42	93.56	99.08	94.43	98.61	96.48	98.92	97.43	98.71	98.06